ACS APPLIED MATERIALS & INTERFACES

Research Article

www.acsami.org

Controlled Synthesis and Catalytic Activity of Copper Sulfide Nanostructured Assemblies with Different Morphologies

Joyjit Kundu and Debabrata Pradhan*

Materials Science Centre, Indian Institute of Technology, Kharagpur, West Bengal 721 302, India

ABSTRACT: A simple, template-free and mild solution chemistry route was employed to synthesize diverse copper sulfide (CuS) nanostructured assemblies at 70 °C by varying the solvent (water or ethylene glycol, or their ratios (3:1, 1:1 and 1:3)). The CuS structures in the shape of spheres and nanotubes were found to be assemblies of either nanoplates or nanoparticles. The nanotube formation was elaborately studied by varying the synthesis parameters such as temperature, reaction duration, precursor's ratio, and counterions. Counterions such as NO_3^- and SO_4^{2-} were found to be suitable for nanotube formation whereas in the presence of Cl^- and OAc^- ions, CuS flake-like and nanoparticle assemblies are obtained, respectively. The optical bandgaps for the CuS with different morphologies were measured to be in the range of 1.88−2.16 eV. The bandgap of CuS in the visible region of electromagnetic radiation prompted it to be used as photocatalyst in the past under natural light. However, we demonstrate here the similar catalytic performance of as-synthesized CuS nanostructures for the degradation of methylene blue in the dark, suggesting that light does not play a role in its catalytic behavior.

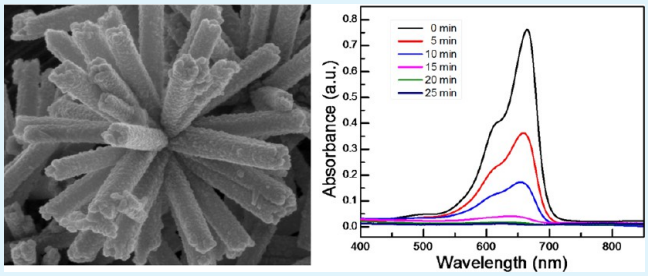

KEYWORDS: *CuS nanotubes, solid spheres, nanoplates, nanoparticles, self-assembly, catalysis*

1. INTRODUCTION

Chalcogenides such as PbS, ZnS, CdS, CuS and Bi_2S_3 are inorganic materials that have been drawing attention of researchers for their unique properties and potential applications.[1−5] Among these materials, copper sulfide (Cu_xS with x = 1−2) is one of the transition metal chalcogenides that exhibits different stoichiometric forms with crystal structure varying from orthogonal to hexagonal. The shape, size, stoichiometric composition and crystal structure usually control the optical and electrical properties of copper sulfide.[6,7] Copper sulfides with five different stoichiometries such as covellite (CuS), anilite ($Cu_{1.75}S$), digenite ($Cu_{1.8}S$), djurlite ($Cu_{1.95}S$) and chalcocite (Cu_2S) are known to be stable at room temperature.[8] These copper sulfides behave as semiconductors with either direct or indirect bandgaps, depending on the stoichiometric ratio of Cu to S. The copper vacancies present in these copper sulfides act as electron acceptors, making them p-type semiconductors.[9] In addition, the copper percentage is known to control the bandgap (E_g) of Cu_xS. The E_g of Cu_xS increases with decrease in the x value (E_g =1.2 eV for Cu_2S, 1.75 eV for $Cu_{1.8}S$ and 2.2 eV for CuS).[10−12] In terms of these E_g values, CuS can absorb maximum solar energy among the Cu_xS. Therefore, it is imminent to synthesize CuS that would find possible applications in the solar cells and other optoelectronic devices. Furthermore, CuS nanocrystals have been found as one of the potential materials for application in catalysis[12,13] biosensor,[14] tissue imaging,[15] drug delivery,[16] Li-ion battery,[17] and memory cell.[18]

Varieties of CuS micro- and nanostructures have been synthesized using solid-state synthesis,[19] sonochemical,[20] hydrothermal,[21] solvothermal,[22] solution based method,[23] template assisted,[24] atomic layer deposition[25] and chemical vapor deposition (CVD)[26] techniques. CuS in the shape of nanoparticles,[15,27] nanotubes,[28] nanowires,[29,30] nanorods,[23] nanoplates,[31] ball-flower,[32] hollow cages[33] and hollow sphere[34] have been synthesized using the above techniques. Among the different types of nanostructures, one-dimensional nanotubes, nanowires and nanorods have attracted the attention of researchers for their unique properties and have become one of the main research topics in recent years.[35,36] In the past, CuS nanotubes and microtubes were mostly synthesized in the presence of templates such as copper nanowires,[28] thiourea complex,[14,37] $Cu(OH)_2$ nanowires[38] and Cu(I)-complexes[39] using solution chemistry routes. The use of a template requires multiple steps, which is time consuming and expensive. It is also difficult to completely remove the template material, which, therefore, affects the purity of the final product. There are only a few reports on the synthesis of CuS tubes without using templates.[40,41] Gong et al. reported CuS microtubes composed of hexagonal nanoflakes and Zhang et al. prepared CuS nanotubes using oleic acid and poly(vinyl pyrrolidone) (PVP) in a microemulsion system without using templates.[40,41]

In this article, we report the preparation of diverse CuS nanostructures using a simple, template-free and single-step solution chemistry route by varying the reaction medium, i.e., either in pure aqueous or alcohol, i.e., ethylene glycol (EG) or

Received: October 30, 2013
Accepted: January 17, 2014
Published: January 17, 2014

   dx.doi.org/10.1021/am404829g | *ACS Appl. Mater. Interfaces* 2014, 6, 1823−1834

Table 1. Detail Experimental Parameters for the Synthesis of Diverse CuS Nanostructures

morphology	precursors (1:1 molar ratio)	solvent	reaction temperature (°C)	duration (h)	bandgap (eV)
CuS microspheres	$Cu(NO_3)_2$ and $Na_2S_2O_3$	water	70	4	2.08
CuS nanotubes	$Cu(NO_3)_2$ and $Na_2S_2O_3$	water−EG (1:3)	70	4	2.06
CuS nanoflakes	$CuCl_2$ and $Na_2S_2O_3$	water−EG (1:3)	70	4	2.16
CuS nanoparticles	$Cu(OAc)_2$ and $Na_2S_2O_3$	water−EG (1:3)	70	4	1.88

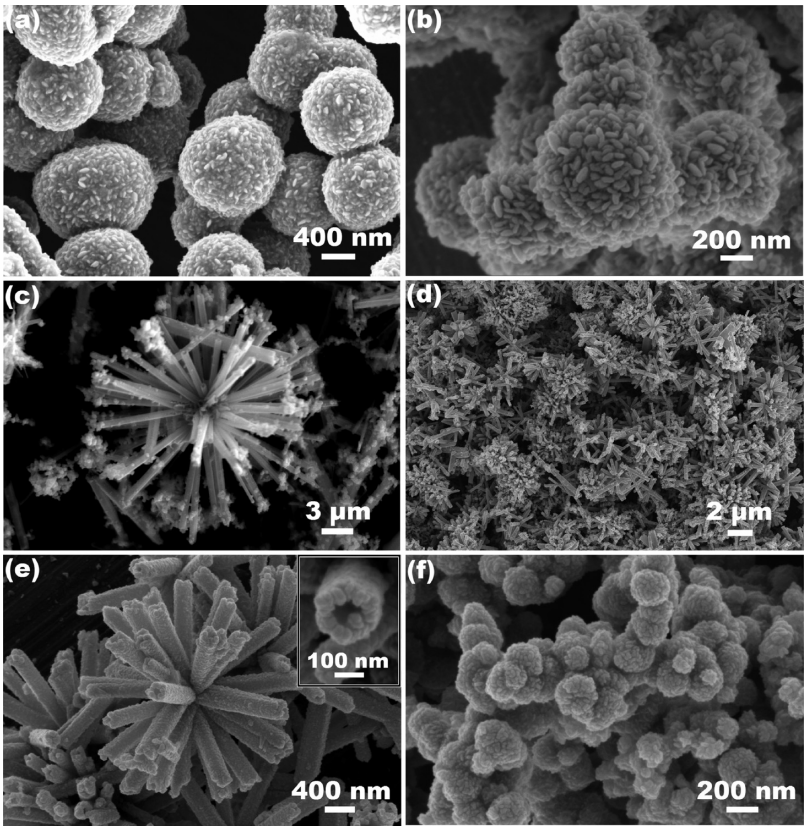

Figure 1. SEM images of solution-based synthesized CuS nanostructures obtained from precursors $Cu(NO_3)_2$:$Na_2S_2O_3$ = 1:1 at 70 °C in 4 h using (a) water, (b) 3:1 water−EG, (c) 1:1 water−EG and (d and e) 1:3 water−EG (f) EG, as solvent.

mixture of these two solvents in different ratios at 70 °C. The main advantages of the present process of synthesizing CuS nanostructure self-assemblies are simpler reagents, lower temperature and shorter duration than that of previous reports.[40,42] Self-assembled CuS nanostructures are normally prepared by a hydrothermal/solvothermal technique. Cheng et al. and Meng et al. recently reported a ball-like morphology and hollow spheres self-assembled of nanoplates using a hydrothermal/solvothermal process, respectively.[32,43] In addition to the CuS spheres self-assembled of either nanoplates or nanoparticles, we report synthesis of CuS nanotubes consisted of nanoparticles. In an optimum solvent ratio (1:3 water−EG), CuS nanotubes were solely obtained. More importantly, the temperature and duration of CuS nanotubes synthesis in the present work is, respectively, lower and faster than that of previous reports.[40,41] The effects of various synthesis parameters such as types of solvent (aqueous and/or alcohol, and their mixture), reaction temperature and duration, precursor concentration and counterions on the formation of CuS nanotubes are investigated in detail. Furthermore, the catalytic activity of as-synthesized CuS nanostructures is studied for the methylene blue (MB) degradation. In the textile industries, synthetic organic dyes are used for coloring the fabrics. As a result, the effluents from these industries contain a high amount of synthetic organic dyes, which cause water contamination. Several oxide materials, including TiO_2, are extensively used as a photocatalyst for dye degradation.[44] However, due to large bandgap of most of the oxide materials, they are not very suitable to be used as a photocatalyst. Efforts have been made to shift the bandgap toward the visible region for practical application.[45] In recent years, CuS has been successfully used for the dye degradation in the presence of visible light and H_2O_2 due to its lower bandgap than that for oxides.[33] In contrast, we herein report for the first time the direct catalytic behavior of CuS by demonstrating the MB degradation in the dark.

2. EXPERIMENTAL DETAILS

2.1. Chemicals. Copper nitrate ($Cu(NO_3)_2·3H_2O$), copper sulfate ($CuSO_4·5H_2O$), copper acetate ($Cu(OAc)_2·H_2O$), sodium thiosulfate ($Na_2S_2O_3·5H_2O$), ethylene glycol (EG), hydrogen peroxide (H_2O_2, 30%) were from Merck, India; copper chloride ($CuCl_2·2H_2O$) and ammonium thiosulfate ($(NH_4)_2S_2O_3$) were from Loba Chemie, India; ethanol was from Changshu Yangyuan Chemical, China. All the above reagents were analytical grade and used without further purification.

2.2. Synthesis. Typically, in a 100 mL round bottom flask, 40 mL of solvent (100% water or 100% EG or their mixture in the ratio of

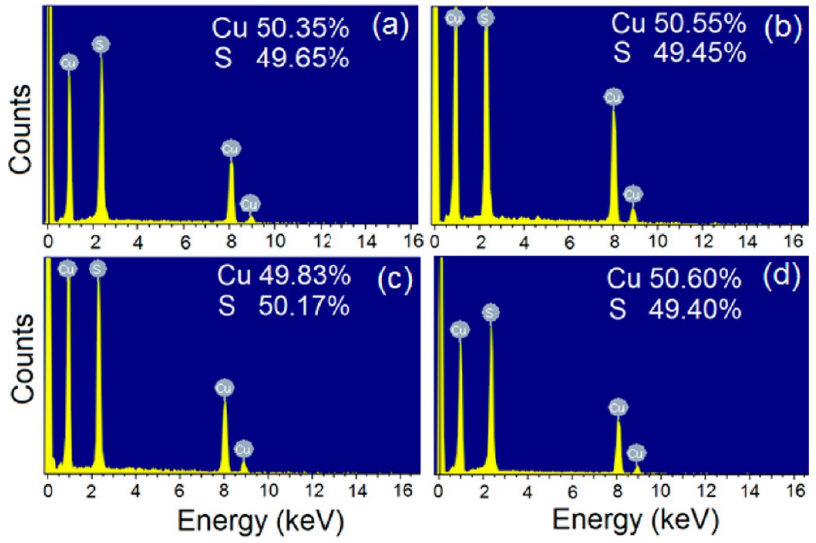

Figure 2. EDX spectra of CuS nanostructures obtained from precursors $Cu(NO_3)_2$:$Na_2S_2O_3$ = 1:1 at 70 °C in 4 h using (a) water, (b) 1:1 water−EG, (c) 1:3 water−EG and (d) EG, as solvent.

3:1, 1:1 or 1:3) was taken. Then 483 mg of $Cu(NO_3)_2$ (2 mmol) and 496 mg of $Na_2S_2O_3$ (2 mmol) were added to above 40 mL solvent (final concentration of Cu^{2+} and $S_2O_3^{2-}$ was 0.05 M). Then the solution was manually stirred to mix the precursors until a yellowish green color solution was obtained. Then the round bottom flask containing solution was placed in an oil bath held at 70 °C and heated for 4 h with constant stirring. After 4 h, the flask was taken out of the oil bath and cooled down to room temperature. The precipitated product was filtered and washed with ethanol and water several times and dried at 60 °C for 4 h prior to characterization. While keeping the water−EG solvent ratio (1:3) fixed, at which CuS nanotubes formed, the reaction temperature was varied in the range of 70−180 °C. Furthermore, the reaction duration was varied from 15 min to 8 h while keeping other parameters fixed. Experiments were also performed with different precursor ($Cu(NO_3)_2$:$Na_2S_2O_3$) molar ratios, i.e., 1:1, 1:2 and 2:1, keeping other parameters constant. The effect of counterions on the formation of CuS nanostructures was studied using five different precursor combination (1) $Cu(NO_3)_2$ and $Na_2S_2O_3$, (2) $CuSO_4$ and $Na_2S_2O_3$, (3) $CuCl_2$ and $Na_2S_2O_3$, (4) $Cu(OAc)_2$ and $Na_2S_2O_3$ and (5) $Cu(NO_3)_2$ and $(NH_4)_2S_2O_3$. The experimental condition for synthesizing different CuS nanostructures is presented in Table 1.

2.3. Characterization. The X-ray diffraction (XRD) measurement was carried out using a PANalytical X'pert pro PW 3040/60 instrument in the 2θ range of 10° to 70°. The surface morphology of as-prepared products was examined with Carl-Zeiss EVO 60 scanning electron microscopy (SEM) attached with an Oxford EDS detector and Carl-Zeiss SUPRA 40 field emission scanning electron microscopy (FESEM). The transmission electron microscopy (TEM) study was performed with a FEI-TECHNI-G^2 instrument at an operating voltage of 200 kV. The optical property of CuS samples was measured with a Perkin-Elmer Lambda 750 UV−Vis spectrophotometer. The photoluminescence (PL) measurements were performed with a SCINCO FluoroMate FS-2 spectrophotometer with an excitation wavelength of 250 nm.

2.4. Catalytic Degradation of MB using CuS Nanostructures. The catalytic activity of different as-synthesized self-assembled CuS nanostructures was studied by MB degradation. First, 10 mg of catalyst powder (CuS nanostructures) was dispersed in 40 mL 2×10^{-5} (M) MB solution in the dark. The MB decomposition was studied after the catalyst−MB mixed solution was stirred for 30 min in the dark for complete adsorption−desorption of MB on the catalyst surface. For the decomposition of MB, 1 mL of H_2O_2 was added to above catalyst−MB mixed solution and the solution was stirred in the dark for different durations. The MB solution was collected after selected durations, and the MB concentration was measured with a Perkin-Elmer Lambda 750 UV−Vis spectrophotometer.

3. RESULTS AND DISCUSSION

3.1. Morphology of CuS Nanostructures. *3.1a. Effect of Solvent Composition.* The morphology of as-synthesized CuS nanostructured materials was examined with SEM. Either aqueous or alcohol (EG) or a mixture of these two solvents was taken at different ratios to observe their effect on the formation of CuS nanostructures while keeping all other parameters such as precursor molar ratio ($Cu(NO_3)_2$:$Na_2S_2O_3$) = 1:1, reaction temperature (70 °C) and reaction duration (4 h) fixed. Figure 1a−f shows the SEM images of CuS nanostructures obtained in different solvent medium, i.e., (a) water, (b) 3:1 water−EG, (c) 1:1 water−EG, (d,e) 1:3 water−EG and (f) EG. In the aqueous medium, the as-synthesized CuS product was found with a spherical morphology of diameter ∼1 μm (Figure 1a). These spheres are actually composed of agglomerated nanoplates of width and length ∼100 nm, and thickness ∼20 nm measured from the magnified SEM images (not shown). In a 3:1 water−EG solvent ratio, the morphology of the product (Figure 1b) is found to remain a spherical shape, consisting of nanoplates. However, the average diameter of the sphere and the size of the nanoplates are reduced to ∼500 nm and <100 nm, respectively. In addition, these nanoplates appear to be loosely agglomerated (Figure 1b) than the former prepared in only aqueous medium (Figure 1a). Previous studies reported CuS spheres were hollow with a large diameter (5−20 μm) prepared at >120 °C with a reaction duration more than 24 h.[46,47] However, Wang et al. reported CuS hollow spheres of an average diameter of 500 nm using CTAB as a surfactant.[48] In all these reports, hollow spheres were reported to be composed of microflakes/nanoplates. In contrast, we obtained solid CuS spheres of much smaller diameter (0.5−1.0 μm) at a lower temperature (70 °C) and in a short duration (4 h) in the absence of a surfactant.

In 1:1 water−EG solvent ratio, the morphology of the product is found to be drastically different to 100% water and 3:1 water−EG. Here we obtained a tube shape morphology (Figure 1c) of the product along with some spheres of ∼400 nm in diameter adhered to the tubes. These submicrometer tubes appear to grow in every direction from one central

nucleation point. The length and diameter of these tubes are in the range of 8−10 μm and 0.5−1 μm, respectively. The wall thickness of these CuS tubes is ∼200 nm. These tubes are found with a hexagonal shape across their body (SEM not shown). With increasing EG in the solvent, i.e., at 1:3 water−EG, we obtained only nanotubes (Figure 1d,e) with uniform length (∼1 μm) and outer diameter (150−200 nm) across the whole product. Figure 1d represents a low magnification SEM image of CuS nanotubes, indicating their uniform length and diameter. Figure 1e shows a magnified SEM image of these nanotubes. A further magnified SEM image (shown as inset in Figure 1e) clearly indicates that CuS nanotubes have an inner diameter of ∼100 nm and are composed with 40−60 nm diameter nanoparticles (verified by TEM, discussed later). In addition, the surface of the CuS nanotubes obtained in this case (i.e., in 1:3 water−EG) appears to be relatively rougher than that obtained with 1:1 water−EG. The previous reports on the CuS nanotubes/microtubes were primarily two-step self-sacrificial template-based synthesis where either Cu(I)−complex,[14,37] Cu nanowires,[28] or $Cu(OH)_2$ nanowires[38] acted as a template. These template-assisted processes produced CuS nanotubes/microtubes of length and diameter in the range of 20−40 μm and 50 nm−1 μm, respectively. Moreover, Zhang et al. prepared CuS nanotubes composed of nanoparticles using a solvothermal technique at 150 °C in 12 h.[41] Unlike the previous works, we demonstrate here the formation of CuS nanotubes by optimizing the solvent medium at a lower temperature (70 °C) using a template-free simple solution route. With 100% EG, the morphology of the product (Figure 1f) was a spherical type with a deformed shape. In addition, unlike the previously obtained spheres made from nanoplates, these deformed spheres are found to consist of nanoparticles. The size of these nanoparticles is measured to be ∼25 nm, which is smaller to the nanoplates of size 50−100 nm obtained with 100% water and 3:1 water−EG solvent media.

Figure 2 shows the energy dispersive X-ray (EDX) spectra of CuS nanostructures, i.e., microspheres (Figure 2a), submicrometer tubes (Figure 2b), nanotubes (Figure 2c), and deformed spheres (Figure 2d) obtained using water, 1:1 water−EG, 1:3 water−EG, and EG, as solvent, respectively. The Cu to S atomic ratio for all these cases is found to be approximately 1:1, confirming stoichiometry of CuS. Additionally, it suggests that the reaction medium does not have any effect on the phase and composition of the product.

We have recently reported the formation mechanism of CuS in 100% water albeit using a hydrothermal method.[49] Similar results, i.e., spherical structures, consisted of nanoplates that have been obtained in the present aqueous solution-based synthesis process, suggesting the same mechanism was involved. However, introducing an optimum quantity of EG into water produces nanotubes and in the presence of only EG solvent, smaller clusters consisting nanoparticles were obtained, as shown in Figure 1f. The formation of CuS in the presence of EG can follow following reaction steps. First, EG can reversibly convert into aldehyde and water in reaction 1 and in the subsequent step (reaction 2) CuS can be produced.

$$HOCH_2CH_2OH \Leftrightarrow CH_3CHO + H_2O \quad (1)$$

$$CH_3CHO + H_2O + 2Cu(NO_3)_2 + Na_2S_2O_3 \rightarrow 2CuS\downarrow + CH_3COOH + 2NaNO_3 + 2HNO_3 \quad (2)$$

The alcohols, such as EG and benzyl alcohol, are known to play the roles of solvent, reducing and/or stabilizing agent in the synthesis of metal, metal oxide and calcogenide nanoparticles.[50−52] The stabilization occurs either directly through OH^- or by intermediate acetate formation.[50,53] The FTIR spectrum (not shown) of as-synthesized CuS nanotubes indicates the stabilization through OH^-.

In the absence of EG (i.e., 100% water), the initial particles were found to be plate-like structures (Figure 1a). As the EG in the reaction medium is increased, the stabilizing effect of EG leads to formation of smaller deformed spheres composed of nanoparticles of much smaller size than that of nanoplates. Upon formation of nanoplates/nanoparticles, they are aggregated to spherical structures to reduce the surface energy. It is important to note that the nucleation and aggregation of nanoparticles are normally slower in a non-aqueous solvent than an aqueous solvent. This is because of fewer surface hydroxyl groups and a higher viscosity of non-aqueous solvent. This allows the self-assemblies to occur at different rates, forming different morphologies in different solvents.[54] The loose agglomeration of nanoparticles in the formation of nanotubes in the present work can therefore be attributed to the higher viscosity of EG. Moreover, the formation of different structures is also driven by the minimization of the total energy of the system. Oriented assembly of Fe_3O_4 nanoparticles into monodisperse hollow single-crystal microspheres has been reported using EG as a reaction medium.[55] The strong chelating ability of EG promotes transition metal complex formation using its hydroxyl group as a ligand.[56] The assemblies of ZnSe and PbS/PbSe nanoparticles/nanoplates to spherical structures have also been reported with a higher EG content in the solvent.[57,58] The formation of different morphologies in the present case can therefore be attributed to the optimum ratio of water to EG, which affects the solubility, reactivity and diffusion behavior of the reagents and the intermediates.[59,60] Figure 3 displays the schematics of CuS morphologies obtained by varying the reaction medium. When the copper nitrate is added to the respective solvent, a bluish transparent solution is obtained, which turns turbid pale or greenish-yellow by adding

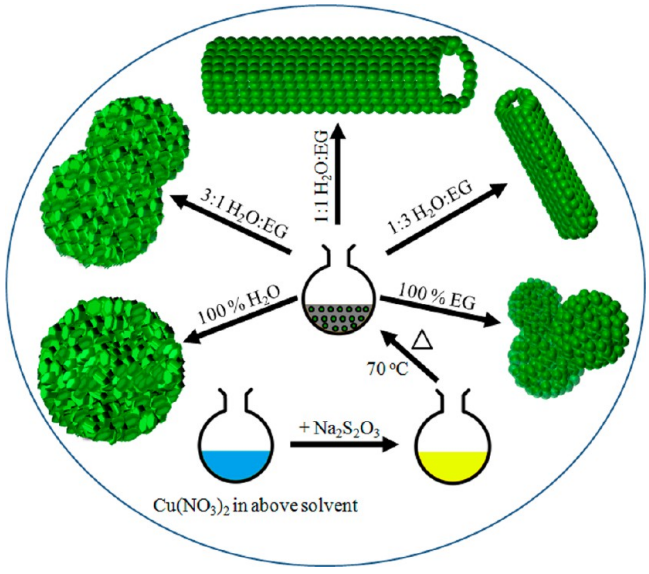

Figure 3. Schematics of formation of different self-assembled CuS nanostructures obtained by varying the ratio of water to EG.

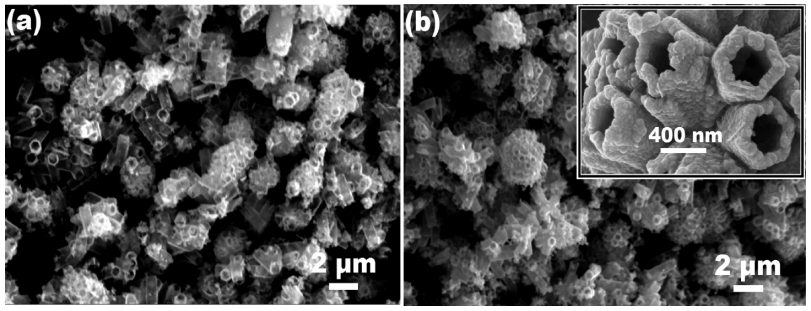

Figure 4. SEM images of solution-based synthesized CuS nanotubes obtained from precursor $Cu(NO_3)_2$:$Na_2S_2O_3$ = 1:1 at (a) 120 °C and (b) 180 °C with 1:3 water−EG solvent in 4 h.

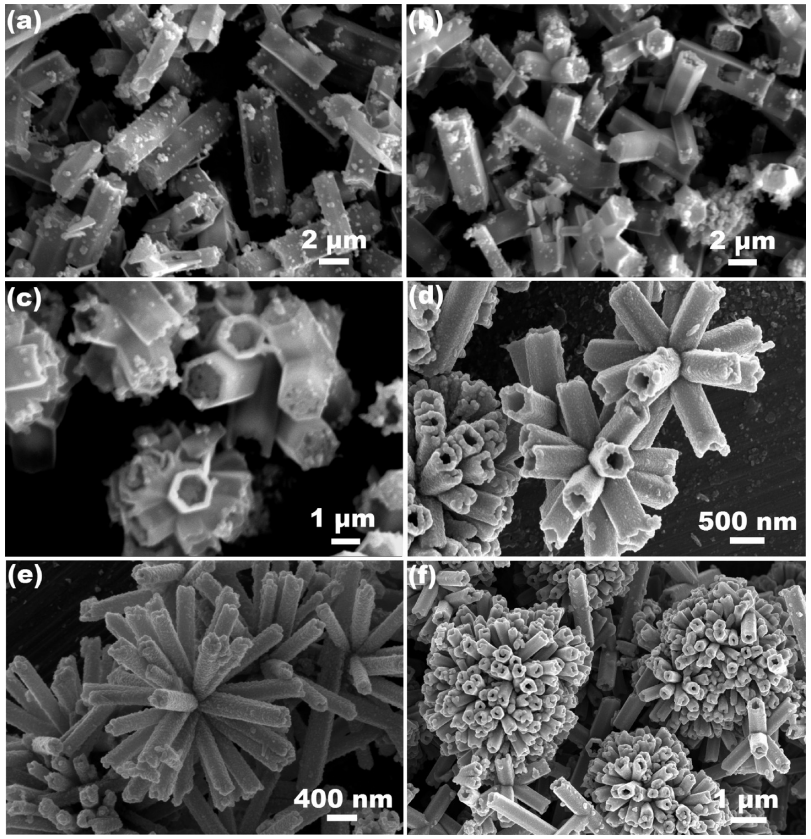

Figure 5. SEM images of solution-based synthesized CuS microrods/nanotubes obtained from precursor $Cu(NO_3)_2$:$Na_2S_2O_3$ = 1:1 at 70 °C with 1:3 water−EG solvent in (a) 15 min, (b) 30 min, (c) 1 h, (d) 2 h, (e) 4 h and (f) 8 h.

sodium thiosulfate. This is due to the formation of a complex, $Na_2(Cu(S_2O_3)_2)$ and $NaNO_3$.[49] This complex produces different morphologies of CuS by heating in different ratios of water−EG solvent at 70 °C. Here, the reaction medium plays an important role in controlling the shape of the basic CuS building blocks in their self-assembling process. In particular, the higher viscosity of EG increases the steric hindrance in reaction system causing reduction of particle sizes of the product,[61] which is obvious in the present case. The greenish-black solid product was finally obtained after heating the $Na_2(Cu(S_2O_3)_2)$ complex for a selected duration and was separated by centrifuge.

3.1b. Effect of Reaction Temperature. Reaction temperature can play a role in the size and shape of nanotubes. There are no previous reports on the optimization of synthesis temperature in the formation of CuS nanotubes. By keeping the optimized solvent ratio (1:3 water−EG) and precursor ratio $Cu(NO_3)_2$:$Na_2S_2O_3$ = 1:1 fixed, the reaction temperature was varied to synthesize CuS nanotubes. Figure 4a,b shows the SEM images of CuS nanotubes obtained at 120 and 180 °C in 4 h, respectively. These nanotubes are found to be quite uniform and hexagonal in shape across their body. With increases in the reaction temperature from 70 to 180 °C, the length of nanotubes remains same (∼1 μm) whereas the average diameter is found to be increased to ∼400 nm (at 120 °C) and ∼500 nm (at 180 °C) from 200 nm (at 70 °C) (Figure 1d,e). It suggests that a lower reaction temperature of 70 °C is suitable to grow smaller diameter CuS nanotubes. This is in support to the previous study by Mao et al., who obtained 50 nm diameter CuS nanotubes at room temperature using a $(Cu(tu))Cl{\cdot}0.5H_2O$ (tu = thiourea) complex as a sacrificial template.[37] The previous reports on larger diameter CuS nanotubes (250−800 nm) are possibly due to the use of a higher synthesis temperature (>80 °C).[14,40]

3.1c. Effect of Reaction Duration. We further investigated the effect of reaction duration to understand the growth mechanism of CuS nanotubes. Experiments were performed separately for reaction durations of 15 min, 30 min, 1 h, 2 h and 8 h, keeping other parameters such as precursor ratio ($Cu(NO_3)_2$: $Na_2S_2O_3$) = 1:1, temperature (70 °C) and water−EG solvent ratio (1:3) fixed. After the reaction was allowed for a specific duration, the reaction vessel was cooled down to room temperature and the product was collected by centrifuge. Figure 5a,b shows the SEM images of CuS microrods obtained in 15 and 30 min of reaction, respectively. The length and diameter of these microrods are measured to be in the range of 5−7 and 1−2 μm, respectively. These microrods are found with a hexagonal shape across the body and a few microrods are joined at the middle producing a cross-sign structure. When the reaction duration is increased to 1 h, a larger number of hexagonal shaped microrods are found be joined together forming clusters (Figure 5c). The length and diameter of the microrods formed after 1 h of reaction are in the range of 3−5 and ∼1 μm, respectively, which is smaller than that of microrods formed after 15 or 30 min of reaction duration. In addition, several of these microrods are found to be hollow toward the axial end. This suggests that the initially formed solid rods are degraded at a higher rate on the axial directions than that of the lateral sides. This degradation produced nanoparticles that appeared on the surface of these microrods (Figure 5a−c). When the reaction duration is increased to 2 h, the hexagonal tube shaped structure clearly emerged with a length and outer (inner) diameter in the range of 0.8−1.5 μm and 300−350 nm (200−250 nm), respectively (Figure 5d). Similar types of tubes are obtained when the reaction duration is increased to 4 (Figure 5e) and 8 h (Figure 5f) but with a shorter length (0.8−1 μm) and smaller diameter (150−200 nm). Two important observations are made on the formation of the CuS structures with increasing the reaction duration. First, the length and diameter of the CuS structures are reduced with increasing the reaction duration. Second, there is a preferential etching on the axial direction to create hollowness in the microrods (Figure 5a), producing nanotubes (Figure 5d−f). In addition, the sharp hexagonal edges (Figure 5a−d) on the microrod's body appear to disappear with increasing the reaction duration to more than 2 h (Figure 5e,f). The structure and composition of the solid rods and tubes was found to be same, i.e., CuS, as analyzed by XRD and EDX (not shown), respectively.

On the basis of the morphologies of CuS structures obtained by varying the reaction durations, a schematic diagram is presented in Figure 6. After the copper and sulfur precursors were stirred in the chosen solvent, the solution color was found to slowly change from blue to greenish-yellow. However, the precipitate was observed only after 15 min of heating and stirring. The solid microrods that formed after 15 min of reaction was the initial morphology (Figure 6a) of the product and a similar type of product was obtained after 30 min (Figure 6b). When the reaction duration was increased to 1 h, the length and diameter of these microrods decreased and were found to be clustered with growth from one central nucleation point to different directions (Figure 6c,d). In addition, there was tube type morphology at the end of these microrods. This suggests that initially formed microrods were etched from all directions at different rates with a faster etching rate on the axial direction. When the reaction duration is increased to 2 h (Figure 6e) and 4 h (Figure 6f), the decrease in length and

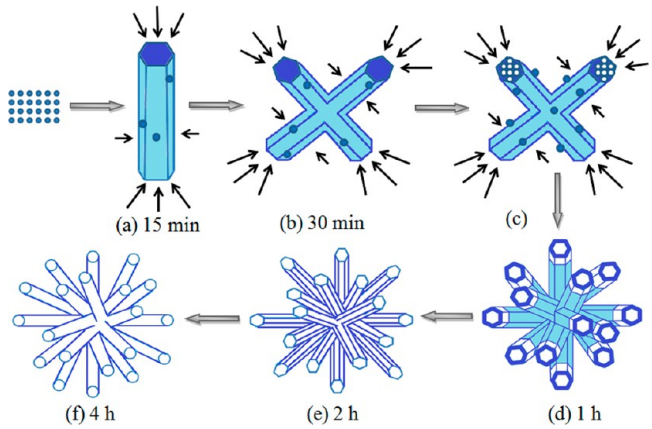

Figure 6. Schematic representation of CuS nanotubes formation as a function of reaction duration.

diameter, improvement in the tube formation, and change in outer tube morphology from hexagonal to round shape strongly suggest etching of the initial product. Further study is underway to understand the detail formation mechanism of CuS nanotubes.

3.1d. Effect of Precursor Ratio. To see the effect of precursor ratios on CuS nanotube formation, three different molar ratios of $Cu(NO_3)_2$ and $Na_2S_2O_3$ (1:1, 2:1 and 1:2) were taken, keeping all other reaction parameters the same (i.e., solvent water−EG = 1:3, reaction temperature 70 °C and reaction duration 4 h). Figures 1e and 7a,b show the morphology of product obtained with $Cu(NO_3)_2$ and $Na_2S_2O_3$ molar ratios of 1:1, 2:1 and 1:2, respectively. The detailed discussion on the formation of CuS nanotubes with 1:1 $Cu(NO_3)_2$:$Na_2S_2O_3$ molar ratio has been outlined in the previous sections (refer to Figures 1e and 5e). With a 2:1 molar ratio of $Cu(NO_3)_2$ and $Na_2S_2O_3$, both CuS nanotubes and nanoparticles were obtained. A SEM micrograph (Figure 7a) clearly reveals that CuS nanotubes consist of loosely held nanoparticles. With a 1:2 $Cu(NO_3)_2$ and $Na_2S_2O_3$ molar ratio, there were no CuS nanotubes or other nanostructures, as shown in Figure 7b. Furthermore, it is important to note that the product obtained with a 1:2 $Cu(NO_3)_2$ and $Na_2S_2O_3$ molar ratio was a mixture of CuS and Cu_2S, as confirmed from the XRD measurement (discussed later). This was supported by the EDX analysis, as shown in the inset of Figure 7b. The Cu to S atomic ratio was measured to be 3:2, which is greater than 1:1 but lower than that of 2:1. This is due to the presence of both CuS and Cu_2S, as confirmed by XRD. The previous report on the effect of precursor ratios on the formation of CuS micro/nanospheres and micrometer size bars consisting of nanoflakes or nanotubes is possibly due to the use thiourea and thioacetamide as sulfur sources.[21,40] Therefore, it can be concluded that not only the precursor ratios but also the types of precursors can have a significant role in the formation of CuS nanostructures.

3.1e. Effect of Counterions. We further study the effect of the counterions on the formation of CuS nanostructures. Five different precursors combinations (1) $Cu(NO_3)_2$ and $Na_2S_2O_3$, (2) $CuSO_4$ and $Na_2S_2O_3$, (3) $CuCl_2$ and $Na_2S_2O_3$, (4) $Cu(OAc)_2$ and $Na_2S_2O_3$ and (5) $Cu(NO_3)_2$ and $(NH_4)_2S_2O_3$ with different counterions were chosen. In all these experiments, the molar ratios of the above precursors were kept constant (i.e., 1:1) along with all other reaction parameters such as water−EG (1:3) solvent, reaction temperature (70 °C) and

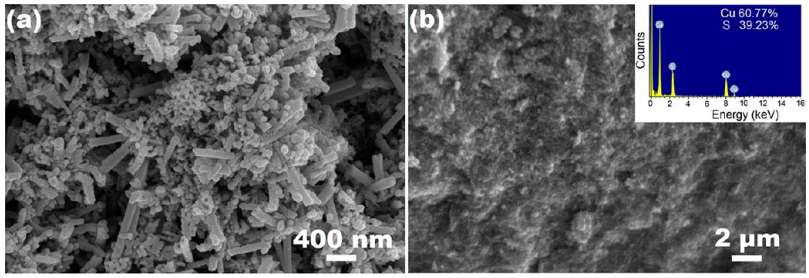

Figure 7. SEM images of solution-based synthesized Cu_xS obtained from precursor (a) $Cu(NO_3)_2$:$Na_2S_2O_3$ = 2:1 and (b) $Cu(NO_3)_2$:$Na_2S_2O_3$ = 1:2 at 70 °C with 1:3 water−EG solvent in 4 h. The Inset shows the EDX spectrum of the corresponding sample.

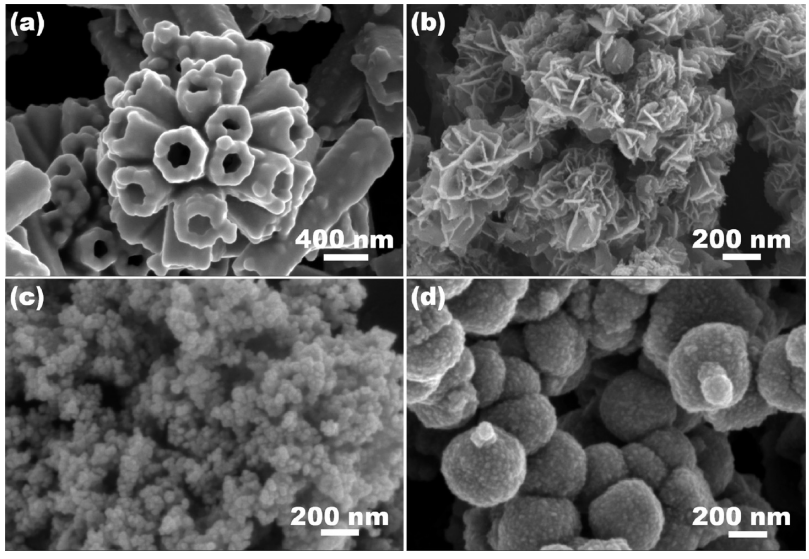

Figure 8. SEM images of solution-based synthesized CuS nanostructures obtained from precursor combinations (a) $CuSO_4$ and $Na_2S_2O_3$, (b) $CuCl_2$ and $Na_2S_2O_3$, (c) $Cu(OAc)_2$ and $Na_2S_2O_3$ and (d) $Cu(NO_3)_2$ and $(NH_4)_2S_2O_3$, in 1:1 molar ratio at 70 °C with 1:3 water−EG solvent in 4 h.

reaction duration (4 h). In the case of $Cu(NO_3)_2$ or $CuSO_4$ with $Na_2S_2O_3$, CuS nanotubes are formed, as shown in Figures 1e and 8a. The diameter of CuS nanotubes formed in the presence of $CuSO_4$ (~400 nm) is found to be larger than that obtained with $Cu(NO_3)_2$ (<200 nm). However, in the presence of a chloride medium ($CuCl_2$ and $Na_2S_2O_3$), no nanotubes were obtained. The structures obtained with $CuCl_2$ and $Na_2S_2O_3$ precursors are the agglomeration of nanoflakes with a thickness <25 nm (Figure 8b). With $Cu(OAc)_2$ and $Na_2S_2O_3$ as copper and sulfur sources, respectively, CuS nanoparticles (Figure 8c) are formed instead of nanotubes or nanoflakes. Interestingly, submicrometer size interconnected spheres were obtained by replacing sodium thiosulfate with ammonium thiosulfate as one of the precursors, along with $Cu(NO_3)_2$. A SEM image (Figure 8d) shows that these spheres consist of fine particles of ~20 nm diameter. From these experiments, it can be concluded that the counterions in the reaction medium play a crucial role in controlling the morphology of the product.

3.2. Crystal Structure and Microstructure. The crystal structure of as-synthesized CuS nanostructures was measured using XRD. Figure 9a presents the XRD pattern of nanotubes (Figure 1d,e) obtained using precursors $Cu(NO_3)_2$:$Na_2S_2O_3$ = 1:1 and 1:3 water−EG solvent at 70 °C for 4 h. The XRD pattern collected in the 2θ range of 10° and 70° shows several diffraction features, which matched a pure hexagonal (covellite) CuS system (JCPDS card No. 006-0464, space group = *P*63/*mmc*(194)). The measured lattice parameters of a = 3.787 Å and c = 16.363 Å were in good accord with the reference data a = 3.792 Å and c = 16.344 Å from JCPDS card No. 006-0464. The products obtained from experiments with varying synthesis parameters (solvent ratio, reaction temperature, reaction duration and counterions) show similar XRD patterns (not shown) with a hexagonal CuS crystal structure. However, the XRD pattern (Figure 9b) of the product (Figure 7b) obtained with precursor molar ratio $Cu(NO_3)_2$:$Na_2S_2O_3$ = 1:2 shows mixed phase of CuS (marked by *) and Cu_2S (marked by ▲)(JCPDS card No. 002-1294). The formation of Cu_2S phase

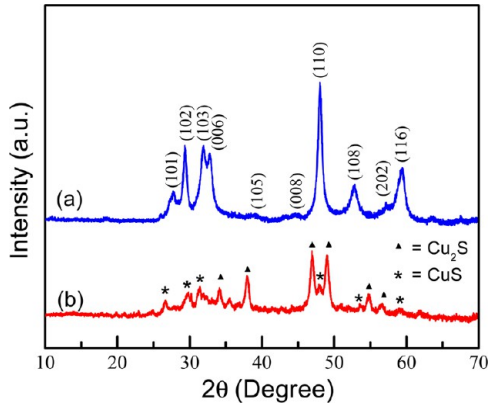

Figure 9. XRD patterns of solution-based synthesized Cu_xS obtained from precursors (a) $Cu(NO_3)_2$:$Na_2S_2O_3$ = 1:1 and (b) $Cu(NO_3)_2$:$Na_2S_2O_3$ = 1:2 with 1:3 water−EG solvent at 70 °C in 4 h.

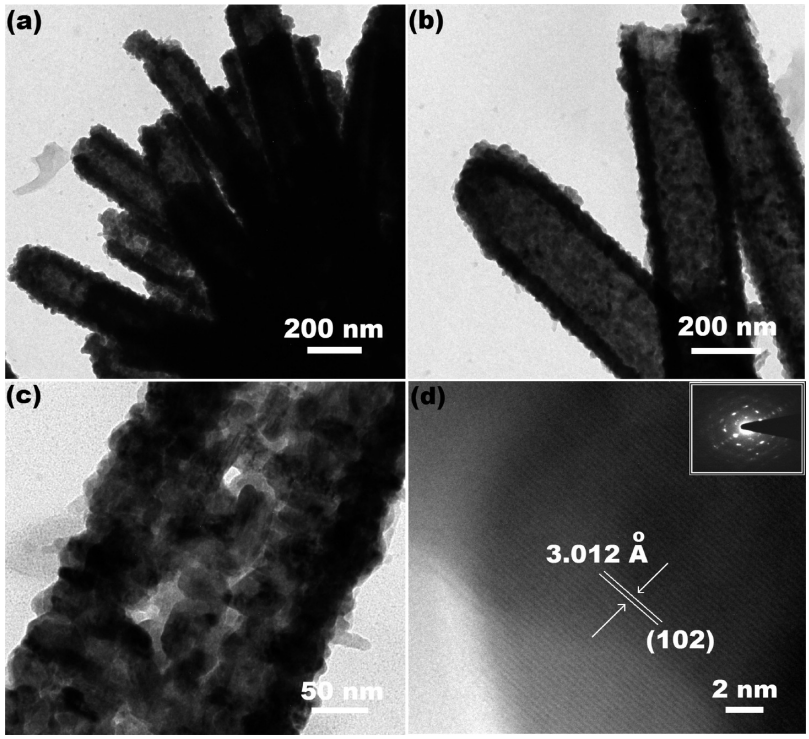

Figure 10. TEM images of (a, b and c) CuS nanotubes obtained from precursor $Cu(NO_3)_2$:$Na_2S_2O_3$ = 1:1 in 1:3 water−EG solvent at 70 °C in 4 h, (d) HRTEM image taken at the edge of a nanoparticle in the CuS nanotube. The inset of d shows the SAED pattern.

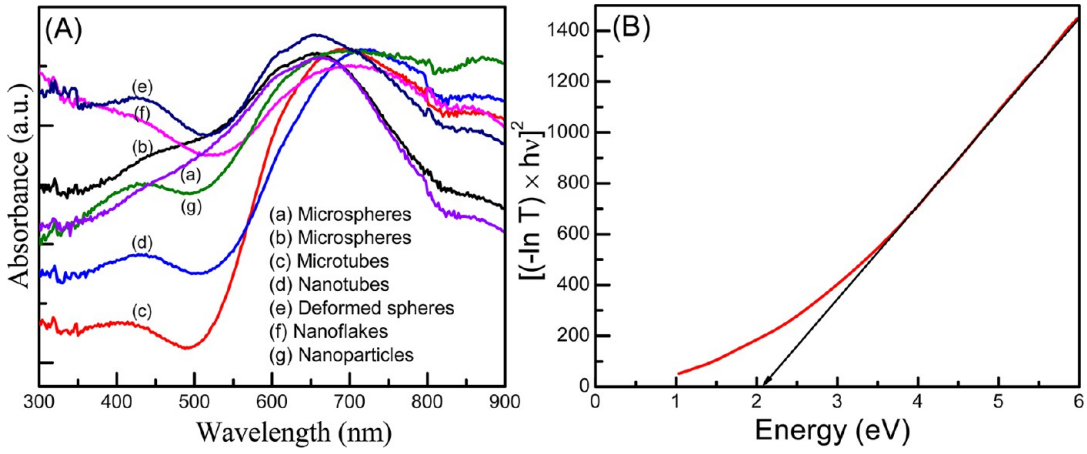

Figure 11. (A) Absorbance vs wavelength plots for CuS microspheres (Figure 1a), microspheres (Figure 1b), microtubes (Figure 1c), nanotubes (Figure 1d,e), deformed spheres (Figure 1f), nanoflakes (Figure 8b) and nanoparticles (Figure 8c). (B) The corresponding bandgap plot for CuS nanotubes is estimated from the zero-crossing value obtained by extrapolation of the linear part to the rising edges of the respective $((-\ln T) \times h\nu)^2$ vs $h\nu$ plots.

is due to the higher percentage of sodium thiosulfate in the reaction medium. As sodium thiosulfate is a reducing agent, its higher concentration is believed to reduce the Cu^{2+} to Cu^{1+}, producing Cu_2S.

The microstructural investigation was carried out using TEM. Figure 10 displays the TEM images of the CuS nanotubes prepared from precursors $Cu(NO_3)_2$:$Na_2S_2O_3$ = 1:1 in 1:3 water−EG solvent at 70 °C in 4 h. A low magnification TEM image (Figure 10a) shows that CuS nanotubes are grown from a central point to different directions as observed in the SEM images (Figure 1d,e). Figure 10b shows both the open- and close-ended CuS nanotubes, in accord with the SEM images. The outer and inner diameters of these nanotubes are measured to be ∼200 and 150 nm, respectively. A magnified TEM image (Figure 10c) indicates that an individual CuS nanotube is composed of elongated nanoparticles of size ∼40−50 nm. Figure 10d shows a high-resolution TEM (HRTEM) image taken at the edge of a CuS nanoparticle in the nanotube. The continuous lattice with a spacing of 3.012 Å is assigned to the (102) plane of a hexagonal CuS crystal. Furthermore, the spot selected area electron diffraction (SAED) pattern (inset of Figure 10d) suggests the single-crystalline nature of individual nanoparticle in the CuS nanotubes.

3.3. Optical Property. The optical property of the CuS samples was measured by a UV−Vis spectrophotometer and

shown in Figure 11. Figure 11A shows the absorbance vs wavelength plots for CuS microspheres (Figure 1a), microspheres (Figure 1b), microtubes (Figure 1c), nanotubes (Figure 1d,e), deformed spheres (Figure 1f), nanoflakes (Figure 8b) and nanoparticles (Figure 8c). It is interesting to note that the absorption spectra show two distinct broad features at ∼425 nm and ∼650−700 nm for the CuS samples (microtubes, nanotubes, nanoparticles, and deformed spheres) self-assembled nanoparticles whereas only one broad peak (at ∼650 nm) for the microspheres self-assembled nanoplates/nanoflakes. The two absorption peaks indicate the zero-dimensional characteristics of corresponding samples,[62,63] with the lower wavelength absorption feature is assigned to the size-quantized particles.[64] Similar UV−Vis absorption spectra with two broad absorptions were reported for CuS spheres, and tubes.[39,65] The FESEM images clearly show that the nanotubes (Figure 1e) and the deformed spheres (Figure 1f) consisted of very fine particle (<50 nm diameter). Therefore, we propose that the particles of much smaller size could be present in these self-assembled structures and thereby they behave as quantum dots. In contrast, an absorption peak at lower wavelengths was not prominent from the samples with the 2-D nanoplates/nanoflakes as basic units.[40] Figure 11B shows the respective representative bandgap plot of $(\alpha h\nu)^2$ vs E $(= h\nu)$ for CuS nanotubes as per Tauc's equation $\alpha h\nu = K(h\nu - E_g)^{1/2}$ for the direct bandgap materials (where $\alpha = -\ln T$, h = plank constant, ν = frequency, K = constant, E_g = bandgap).[66−68] The estimated bandgap at the zero-crossing of linear part of $(\alpha h\nu)^2$ vs $h\nu$ curve is 2.06 eV for the CuS nanotubes. The bandgap for CuS microspheres, nanoflakes and nanoparticles are measured to be 2.08, 2.16 and 1.88 eV, respectively. The estimated bandgap energies are found to be within the reported values for the CuS.[12] Due to the broad absorption, sharp transition was not obtained for the bandgap measurement as shown in Figure 11B. However, on the basis of maximum intensity absorption position and from linear extrapolation of $(\alpha h\nu)^2$ vs $h\nu$ plots, the bandgaps of as-synthesized samples were measured. Our results indicate that morphology have slight effect on the bandgap as summarized in the Table 1.

Figure 12 shows the room temperature PL spectra of CuS samples with different morphologies. In all cases, two broad emission features were obtained, an intense peak in the range of 345−350 nm and a low intensity peak in the range of 450−460 nm. Previous reports suggest that CuS gives a broad spectrum in the range of 400−460 nm.[29,30] The intense broad peak at ∼350 nm is blue shifted as compared with that of the emission in the range of 388−440 nm previously reported for CuS.[69,70] Kumar et al. found a clear blue shift of the emission wavelength with decreasing excitation wavelength.[69] The lower excitation wavelength (250 nm) in the present study could be a factor for emission at a lower wavelength. However, the luminescence behavior of CuS self-assembled nanostructures is not well established and needs further investigation.

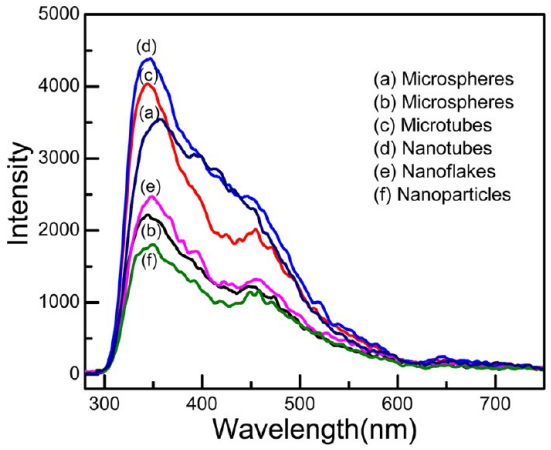

Figure 12. PL spectra of CuS microspheres (Figure 1a), microspheres (Figure 1b), microtubes (Figure 1c), nanotubes (Figure 1d,e), nanoflakes (Figure 8b) and nanoparticles (Figure 8c).

4. CATALYTIC ACTIVITY OF CuS NANOSTRUCTURES

The catalytic activity of the as-synthesized CuS nanostructures was tested for MB degradation in the presence of H_2O_2 in the dark. Unlike the previous reports that CuS act as a photocatalyst (under light irradiation) in the presence of H_2O_2,[33,71] we demonstrate here, for the first time, that light is not a requirement for the catalytic dye degradation. For the catalysis study, 40 mL of 2×10^{-5} (M) MB solution was taken in a beaker and 10 mg of CuS powder was added to it. The resulting solution was stirred while keeping away from the light source and then the solution was centrifuged to separate the CuS. Figure 13a shows the UV−Vis absorption spectra of MB solution stirred with CuS nanotubes at different durations in the dark. The decrease in the absorption at ∼664 nm is due to the adsorption of MB on the CuS surface, which is found to be saturated in 30 min. Then, we added 1 mL of H_2O_2 to a catalyst (different CuS nanostructures) mixed MB solution (i.e., after 30 min) and the solution was stirred in the dark. Figure 13b shows the UV−Vis spectra of MB solution in the presence of H_2O_2 and CuS nanotubes at different durations after originally being kept under dark to saturate the adsorption−desorption of MB on the catalyst surface. The decrease in MB absorbance (Figure 13b) indicates its degradation due to the catalytic nature of CuS nanotubes. It must be noted here that there is a negligible decrease in the absorbance of MB in the presence of only H_2O_2 without the CuS catalyst, as shown in Figure 13c.[33] Figure 13c also displays the MB degradation activity of different CuS nanostructures by plotting C_t/C_0 as a function of time. Here C_0 and C_t are the initial concentration and concentration of MB at time t, respectively. The stability of CuS nanotubes catalyst was further studied by repeating the MB degradation with same CuS nanotubes sample upon adding 1 mL of H_2O_2 in each cycle. Figure 13(d) shows the plot of degradation percentage as a function of cycle number. The catalytic performance was found to be decreased to 94.5% after four cycles, which is higher than that reported from cubic CuS cages and hierarchical hollow spheres in the presence of natural light and H_2O_2.[33,71] For comparison, we also performed same experiments under dark and in the presence of visible light. A slightly higher MB degradation (∼2−3 %) was found initially in the presence of light as compared to dark and becomes almost equal after 15 min. Table 2 presents the degradation performance of MB as a function of time under dark and in the presence of light using CuS nanotubes or microspheres as a catalyst with H_2O_2. Unlike the previous reports, we demonstrate here that light is not required for MB degradation in the presence of H_2O_2 and therefore CuS simply acts as a catalyst instead of a photocatalyst.

The morphology of CuS nanostructures is found to have an insignificant effect on the MB degradation. The MB is found to

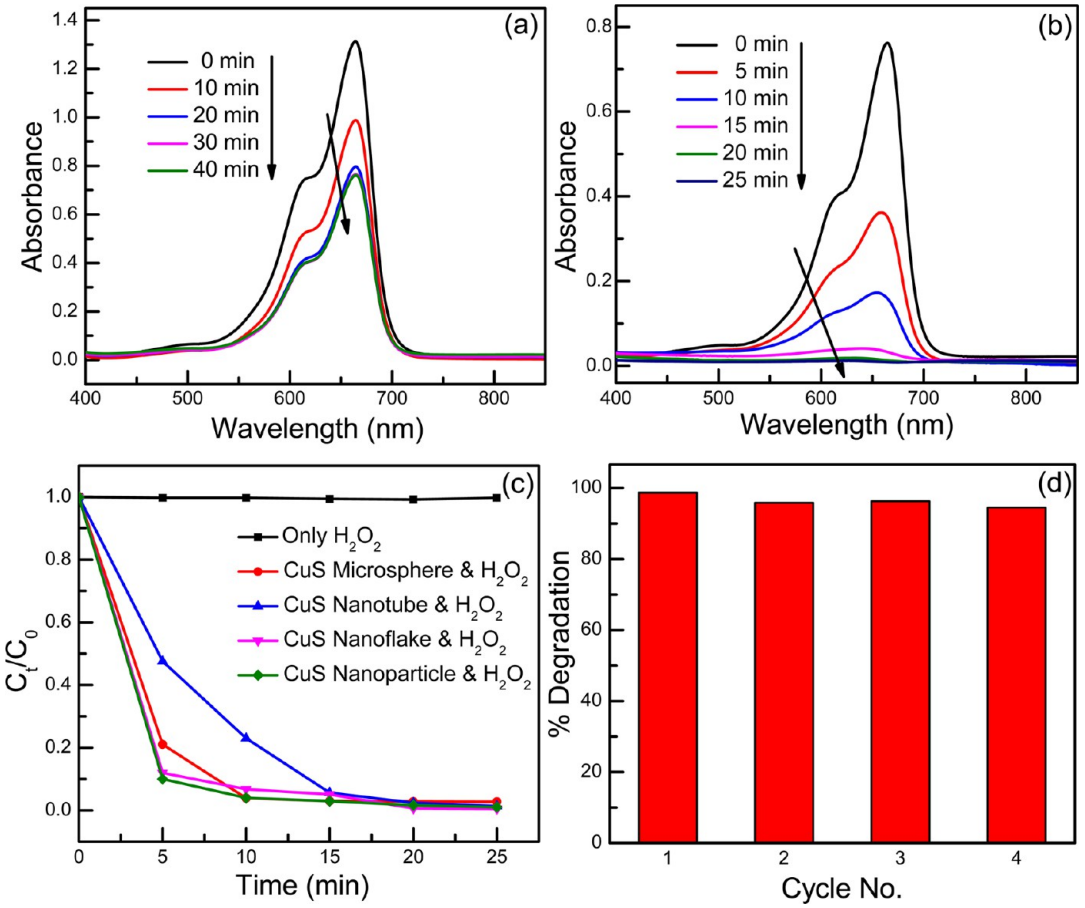

Figure 13. (a) UV−Vis absorption spectra of MB solution at different durations upon adding CuS nanotubes, (b) UV−Vis absorption spectra of MB aqueous solution in the presence of CuS nanotubes after adding 1 mL of H_2O_2. H_2O_2 was added to MB solution after 30 min of stirring with CuS nanotubes only to saturate MB adsorption−desorption on the CuS surface. (c) The MB degradation rate in the presence of only H_2O_2, CuS microspheres and H_2O_2, CuS nanotubes and H_2O_2, CuS nanoflakes and H_2O_2 and CuS nanoparticles and H_2O_2. (d) The % degradation vs cycle number suggesting the stability of CuS nanotubes for MB degradation. All the measurements were carried out in the dark.

Table 2. Comparison of MB Degradation (in %) in the Dark and in the Presence of Light Using CuS Nanotubes and Microspheres with H_2O_2

duration (min)	CuS nanotubes (dark) (%)	CuS nanotubes (light) (%)	CuS microspheres (dark) (%)	CuS microspheres (light) (%)
5	52.4	54.9	79.0	82.2
10	77.0	82.9	96.1	97.3
15	94.4	92.8	97.1	98.0
20	97.6	97.4	97.2	98.4
25	98.6	98.3	97.3	98.5

be completely degraded in 20 min with CuS of any morphology. The MB degradation mechanism can therefore be ascribed to the formation of hydroxide radicals in the presence of CuS and H_2O_2.[72] The hydroxyl radicals, in turn, react with organic substrate such as MB to degrade. Figure 14 shows the schematic of MB degradation in the presence of H_2O_2 under dark.

$$H_2O_2 \xrightarrow{CuS} HO^{\cdot}$$

$$RH + HO^{\cdot} \rightarrow R^{\cdot} + H_2O \ (RH = \text{organic substrates such as MB})$$

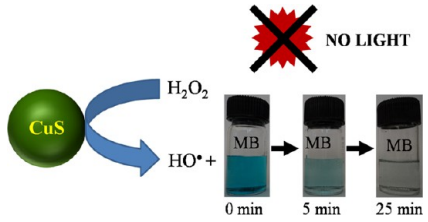

Figure 14. Schematic of MB degradation as a function of time after adding 1 mL of H_2O_2 to the CuS dispersed MB solution under dark.

5. CONCLUSIONS

Submicrometer range CuS spheres and CuS nanotubes consisting of nanoparticles/nanoplates are synthesized using a simple solution chemistry route at low temperature (70 °C). The effect of synthesis parameters such as solvent (water to EG) ratios, reaction temperature and duration, precursors (copper nitrate and sodium thiosulfate) ratios and counterions on the shape, size and structures of CuS nanostructures is studied into the details. The 1:1 $Cu(NO_3)_2$:$Na_2S_2O_3$ precursor ratio and 1:3 water−EG solvent ratio is found to be optimum for producing CuS nanotubes. With increases in the reaction temperature from 70 to 180 °C, diameter of CuS nanotubes is increased from 150−200 to 400−500 nm. The reaction duration also plays an important role in the formation of

dx.doi.org/10.1021/am404829g | ACS Appl. Mater. Interfaces 2014, 6, 1823−1834

CuS nanotubes. Initially (after 15/30 min of reaction), CuS microrods of hexagonal cross-section are formed, which are subsequently evolved to the nanotubes of circular cross-section after 4 h. CuS nanostructures are further synthesized using precursors with different counterions. It is important to note that CuS nanotubes are obtained only with the counterions NO_3^-, and SO_4^{2-} in the presence of Na^+. The bandgap energies are measured to be 2.08, 2.06, 2.16, and 1.88 eV for the CuS spheres, nanotubes, nanoflakes and nanoparticles, respectively. Furthermore, we report here another important finding on the CuS as a catalyst (not a photocatalyst) for MB degradation with high degradation efficiency.

AUTHOR INFORMATION

Corresponding Author

*D. Pradhan. E-mail: deb@matsc.iitkgp.ernet.in.

Notes

The authors declare no competing financial interest.

ACKNOWLEDGMENTS

This work was supported by Department of Science and Technology, New Delhi, India through the grant INT/Korea/P-02. Authors also acknowledge the Central Research Facility (CRF), IIT-Kharagpur for the XRD, SEM and TEM characterizations.

REFERENCES

(1) Moreels, I.; Lambert, K.; Smeets, D.; Muynck, D. D.; Nollet, T.; Martins, J. C.; Vanhaecke, F.; Vantomme, A.; Delerue, C.; Allan, G.; Hens, Z. *ACS Nano* **2009**, *3*, 3023−3030.

(2) Yu, X.; Yu, J.; Cheng, B.; Huang, B. *Chem. − Eur. J.* **2009**, *15*, 6731−6739.

(3) Muruganandham, M.; Kusumoto, Y.; Okamoto, C.; Muruganandham, A.; Abdulla-Al-Mamun, Md.; Ahmmad, B. *J. Phys. Chem. C* **2009**, *113*, 19506−19517.

(4) Kriegel, I.; Jiang, C.; Rodríguez-Fernández, J.; Schaller, R. D.; Talapin, D. V.; da Como, E.; Feldmann, J. *J. Am. Chem. Soc.* **2012**, *134*, 1583−1590.

(5) Tahir, A. A.; Ehsan, M. A.; Mazhar, M.; Wijayantha, K. G. U.; Zeller, M.; Hunter, A. D. *Chem. Mater.* **2010**, *22*, 5084−5092.

(6) Zhao, Y.; Pan, H.; Lou, Y.; Qiu, X.; Zhu, J. J.; Burda, C. *J. Am. Chem. Soc.* **2009**, *131*, 4253−4261.

(7) Takase, K.; Koyano, M.; Shimizu, T.; Makihara, K.; Takahashi, Y.; Takano, Y.; Sekizawa, K. *Solid State Commun.* **2002**, *123*, 531−534.

(8) Zhang, D.-F.; Zhang, H.; Shang, Y.; Guo, L. *Cryst. Growth Des.* **2011**, *11*, 3748−3753.

(9) de Tacconi, N. R.; Rajeshwar, K.; Lenza, R. O. *J. Phys. Chem.* **1996**, *100*, 18234−18239.

(10) Wu, Y.; Wadia, C.; Ma, W.; Sadtler, B.; Alivisatos, A. P. *Nano Lett.* **2008**, *8*, 2551−2555.

(11) Reijnen, L.; Meester, B.; Goossens, A.; Schoonman, J. *Mater. Sci. Eng., C* **2002**, *19*, 311−314.

(12) Basu, M.; Sinha, A. K.; Pradhan, M.; Sarkar, S.; Negishi, Y.; Pal, T. *Environ. Sci. Technol.* **2010**, *44*, 6313−6318.

(13) Zhang, J.; Yu, J.; Zhang, Y.; Li, Q.; Gong, J. R. *Nano Lett.* **2011**, *11*, 4774−4779.

(14) Liu, J.; Xue, D. *J. Mater. Chem.* **2011**, *21*, 223−228.

(15) Ku, G.; Zhou, M.; Song, S.; Huang, Q.; Hazle, J.; Li, C. *ACS Nano* **2012**, *6*, 7489−7496.

(16) Ramadan, S.; Guo, L.; Li, Y.; Yan, B.; Lu, W. *Small* **2012**, *8*, 3143−3150.

(17) Chen, Y.; Davoisne, C.; Tarascon, J.-M.; Guéry, C. *J. Mater. Chem.* **2012**, *22*, 5295−5299.

(18) Ngo, M. V.; Lopatin, S. D.; Pangrle, S. K.; Tripasa, N. H.; Pham, H. T. U.S. Patent 6,746,971 B1, June 8, 2004.

(19) Wang, W.; Ao, L. *Mater. Chem. Phys.* **2008**, *109*, 77−81.

(20) Wang, H.; Zhang, J.; Zhao, X.; Xu, S.; Zhu, J. *Mater. Lett.* **2002**, *55*, 253−258.

(21) Qin, A.-M.; Fang, Y.-P.; Ou, H.-D.; Liu, H.-Q.; Su, C.-Y. *Cryst. Growth Des.* **2005**, *5*, 855−860.

(22) Gorai, S.; Ganguli, D.; Chaudhuri, S. *Cryst. Growth Des.* **2005**, *5*, 875−877.

(23) Roy, P.; Mondal, K.; Srivastava, S. K. *Cryst. Growth Des.* **2008**, *8*, 1530−1534.

(24) Mao, G.; Dong, W.; Kurth, D. G.; Möhwald, H. *Nano Lett.* **2004**, *4*, 249−252.

(25) Johansson, J.; Kostamo, J.; Karppinen, M.; Niinistö, L. *J. Mater. Chem.* **2002**, *12*, 1022−1026.

(26) Xu, M.; Wu, H.; Da, P.; Zhao, D.; Zheng, G. *Nanoscale* **2012**, *4*, 1794−1799.

(27) An, C.; Wang, S.; He, J.; Wang, Z. *J. Cryst. Growth* **2008**, *310*, 266−269.

(28) Wu, C.; Yu, S. H.; Chen, S.; Liu, G.; Liu, B. *J. Mater. Chem.* **2006**, *16*, 3326−3331.

(29) Roy, P.; Srivastava, S. K. *Cryst. Growth Des.* **2006**, *6*, 1921−1926.

(30) Zhang, F.; Wong, S. S. *Chem. Mater.* **2009**, *21*, 4541−4554.

(31) Wu, H.; Chen, W. *Nanoscale* **2011**, *3*, 5096−5102.

(32) Cheng, Z.; Wang, S.; Wang, Q.; Geng, B. *CrystEngComm* **2010**, *12*, 144−149.

(33) Sun, S.; Song, X.; Kong, C.; Deng, D.; Yang, Z. *CrystEngComm* **2012**, *14*, 67−70.

(34) Leidinger, P.; Popescu, R.; Gerthsen, D.; Lünsdorf, H.; Feldmann, C. *Nanoscale* **2011**, *3*, 2544−2551.

(35) Sun, L.; Banhart, F.; Krasheninnikov, A. V.; Rodriguez-Manzo, J. A.; Terrones, M.; Ajayan, P. M. *Science* **2006**, *312*, 1199−1202.

(36) Panda, A. B.; Glaspell, G.; El-Shall, M. S. *J. Am. Chem. Soc.* **2006**, *128*, 2790−2791.

(37) Mao, J.; Shu, Q.; Wen, Y.; Yuan, H.; Xiao, D.; Choi, M. M. F. *Cryst. Growth Des.* **2009**, *9*, 2546−2548.

(38) Liu, X. L.; Zhu, Y. J. *Mater. Lett.* **2011**, *65*, 1089−1091.

(39) Yao, Z.; Zhu, X.; Wu, C.; Zhang, X.; Xie, Y. *Cryst. Growth Des.* **2007**, *7*, 1256−1261.

(40) Gong, J. Y.; Yu, S. H.; Qian, H. S.; Luo, L. B.; Liu, X. M. *Chem. Mater.* **2006**, *18*, 2012−2015.

(41) Zhang, X.; Wang, G.; Gu, A.; Wei, Y.; Fang, B. *Chem. Commun.* **2008**, 5945−5947.

(42) Xu, K.; Ding, W. *Mater. Lett.* **2008**, *62*, 4437−4439.

(43) Meng, X.; Tian, G.; Chen, Y.; Zhai, R.; Zhou, J.; Shi, Y.; Cao, X.; Zhou, W.; Fu, H. *CrystEngComm.* **2013**, *15*, 5144−5149.

(44) Roy, N.; Sohn, Y.; Pradhan, D. *ACS Nano* **2013**, *7*, 2532−2540.

(45) Irie, H.; Watanabe, Y.; Hashimoto, K. *J. Phys. Chem. B* **2003**, *107*, 5483−5486.

(46) Ge, L.; Jing, X.-Y.; Wang, J.; Jamil, S.; Liu, Q.; Song, D.-L.; Wang, J.; Xie, Y.; Yang, P.-P.; Zhang, M.-L. *Cryst. Growth Des.* **2010**, *10*, 1688−1692.

(47) Wan, S.; Guo, F.; Shi, L.; Peng, Y.; Liu, X.; Zhang, Y.; Qian, Y. *J. Mater. Chem.* **2004**, *14*, 2489−2491.

(48) Wang, Y.; Li, Q.; Nie, M.; Li, X.; Li, Y.; Zhong, X. *Nanotechnology* **2011**, *22*, 305401.

(49) Kundu, J.; Pradhan, D. *New J. Chem.* **2013**, *37*, 1470−1478.

(50) Yang, J.; Deivaraj, T. C.; Too, H.-P.; Lee, J. Y. *Langmuir* **2004**, *20*, 4241−4245.

(51) Buha, J.; Arcon, D.; Niederberger, M.; Djerdj, I. *Phys. Chem. Chem. Phys.* **2010**, *12*, 15537−15543.

(52) Zhu, J.-F.; Zhu, Y.-J. *J. Phys. Chem. B* **2006**, *110*, 8593−8597.

(53) Xie, X.; Shang, P.; Liu, Z.; Lv, Y.; Li, Y.; Shen, W. *J. Phys. Chem. C* **2010**, *114*, 2116−2123.

(54) Banfield, J. F.; Welch, S. A.; Zhang, H.; Ebert, T. T.; Penn, R. L. *Science* **2000**, *289*, 751−754.

(55) Yu, D.; Sun, X.; Zou, J.; Wang, Z.; Wang, F.; Tang, K. *J. Phys. Chem. B* **2006**, *110*, 21667−21671.

(56) Chen, J.; Herricks, T.; Geissler, M.; Xia, Y. *J. Am. Chem. Soc.* **2004**, *126*, 10854−10855.

(57) Zhang, L.; Yang, H.; Yu, J.; Shao, F.; Li, L.; Zhang, F.; Zhao, H. *J. Phys. Chem. C* **2009**, *113*, 5434−5443.

(58) Jin, R.; Chen, G.; Pei, J. *J. Phys. Chem. C* **2012**, *116*, 16207−16216.
(59) Ma, Y.-L.; Zhang, L.; Cao, X.-F.; Chen, X.-T.; Xue, Z.-L. *CrystEngComm* **2010**, *12*, 1153−1158.
(60) Zhou, Y.-X.; Yao, H.-B.; Zhang, Q.; Gong, J.-Y.; Liu, S.-J.; Yu, S.-H. *Inorg. Chem.* **2009**, *48*, 1082−1090.
(61) Marques, V. S.; Cavalcante, L. S.; Sczancoski, J. C.; Alcântara, A. F. P.; Orlandi, M. O.; Moraes, E.; Longo, E.; Varela, J. A.; Siu Li, M.; Santos, M. R. M. C. *Cryst. Growth Des.* **2010**, *10*, 4752−4768.
(62) Gondar, J. L.; Cipolatti, R.; Marques, G. E. *Braz. J. Phys.* **2006**, *36*, 960−962.
(63) Khatei, J.; Sandeep, C. S. S.; Philip, R.; Rao, K. S. R. K. *Appl. Phys. Lett.* **2012**, *100*, 081901.
(64) Haram, S. K.; Mahadeshwar, A. R.; Dixit, S. G. *J. Phys. Chem.* **1996**, *100*, 5868−5873.
(65) Mu, C.-F.; Yao, Q.-Z.; Qu, X.-F.; Zhou, G.-T.; Li, M.-L.; Fu, S.-Q. *Colloids Surf., A* **2010**, *371*, 14−21.
(66) Tauc, J.; Menth. *J. Non-Cryst. Solids* **1972**, *8-10*, 569−585.
(67) Pradhan, D.; Leung, K. T. *J. Phys. Chem. C* **2008**, *112*, 1357−1364.
(68) Sapkal, R. T.; Shinde, S. S.; Babar, A. R.; Moholkar, A. V.; Rajpure, K. Y.; Bhosale, C. H. *Mater. Express* **2012**, *2*, 64−70.
(69) Kumar, P.; Gusain, M.; Nagarajan, R. *Inorg. Chem.* **2011**, *50*, 3065−3070.
(70) Zhang, H.; Zhang, Y.; Yu, J.; Yang, D. *J. Phys. Chem. C* **2008**, *112*, 13390−13394.
(71) Jiang, D.; Hu, W.; Wang, H.; Shen, B.; Deng, Y. *Chem. Eng. J. (Amsterdam, Neth.)* **2012**, *189−190*, 443−450.
(72) Mi, L.; Wei, W.; Zheng, Z.; Gao, Y.; Liu, Y.; Chen, W.; Guan, X. *Nanoscale* **2013**, *5*, 6589−6598.